



EXPERIMENTAL AND NUMERICAL INVESTIGATIONS ON THE RESIDUAL STRAINS OF YAG PHASE IN DIRECTIONALLY SOLIDIFIED EUTECTIC AL₂O₃/YAG CERAMIC COMPOSITE

J. J. Sha^a, S. Ochiai^a, S. Iwamoto^b, K. Morishita^b, H. Okuda^a, Y. Waku^c, N. Nakagawa^c,
A. Mitani^c, M. Sato^c and T. Ishikawa^c

^aInternational Innovation Center, Kyoto University, Yoshida, Sakyo-ku,
Kyoto 606-8501, Japan

^bDepartment of Materials Science and Engineering, Kyoto University, Yoshida, Sakyo-ku,
Kyoto 606-8501, Japan

^cUbe Industries Ltd., Ube, Yamaguchi 755-8633, Japan

Keywords: *ceramic composite, residual strains, X-ray diffraction, finite element simulation*

Abstract

Because of the attractiveness in superior oxidation resistance, high stability of the microstructure and excellent high temperature mechanical properties in oxidative environment, directionally solidified eutectic (DSE) oxide/oxide ceramic composite have been considered as one of the most potential structural materials for advanced energy generation systems and space propulsion systems. However, due to the mismatch in coefficient of thermal expansion (CTE), the residual strains are always generated from the fabrication process and thermal cycling in use, which would have an influence on properties of DSE ceramic composites. Therefore, the investigation of magnitude, state and distribution of residual strains in oxide ceramic composites is a crucial work.

In this study, the residual strains of YAG phase in directionally solidified eutectic Al₂O₃/Y₃Al₅O₁₂ (YAG) ceramic composite were estimated by X-ray diffraction technique and finite element method (FEM). In the X-ray strain measurement, the YAG skeleton specimen derived from the composite by removing the Al₂O₃ phase was used as un-strained reference specimen. The X-ray strain measurements with CuK α irradiation were performed on the two faces: parallel and perpendicular to the solidification direction. The principal residual strains measured from the family of 888 diffraction in YAG phase indicated that YAG phase in composite is in compression. The measured residual strains are varied from $-2.19 \pm 0.32 (\times 10^{-4})$ to $-4.22 \pm 0.08 (\times 10^{-4})$ on faces parallel and

perpendicular to the solidification direction respectively. The experimental results were accounted for by the FEM simulation.

1 Introduction

Directionally solidified eutectic (DSE) oxide/oxide ceramic composites possess superior oxidation resistance, high stability of the microstructure and excellent high temperature mechanical properties [1-2]. Thus, DSE oxide/oxide ceramic composites have received considerable attention and been regarded as one of the most potential structural materials for advanced energy generation systems and space propulsion systems.

Since DSE ceramic composites are generally fabricated and expected to be applied in very high temperature environment, the generation of residual stresses due to mismatch of coefficient of thermal expansion (CTE) on cooling during fabrication or during use under thermal cycling is a problem which need to be clarified. On the other hand, the eutectic microstructure and crystallography are varied with the process condition [3-4]. This process-dependent eutectic microstructure and crystallography may result in an influence on the distribution of residual strains in each constituent phase. Therefore, an understanding of the magnitude, state and distribution of residual strains in DSE composite is essential not only for the optimization of fabrication process and application condition, but also for the machinability and use in electronic devices [5].

Extensive efforts have been made to characterize the residual stress in ceramic composites both experimentally and theoretically. Previous studies using X-ray diffraction technique have successfully demonstrated the presence of GPa-level residual stress in some DSE ceramic composites ($\text{Co}_{1-x}\text{Ni}_x/\text{ZrO}_2(\text{CaO})$, NiO-ZrO_2 and so on) [6-8]. Such high residual stresses were caused by the large difference in CTE between/among the constituents and the strong interface.

On the other hand, in the DSE $\text{Al}_2\text{O}_3/\text{Y}_3\text{Al}_5\text{O}_{12}$ (YAG) composite, the difference in CTE between the two constituent phases is very small compared to that in other oxide composites [9]. It is noted that this composite has a clean and strongly constrained interface between two constituent phases without glass phase [10], as well as that in the composites mentioned above. These characteristics make the $\text{Al}_2\text{O}_3/\text{YAG}$ composite to be a potential material in a number of engineering applications, such as structural components for high temperature technologies and electronic devices for high-power white-LED light sources [1-2,5].

In the present work, the X-ray diffraction technique and finite element method (FEM) were applied, to estimate the residual strains in YAG phase of DSE $\text{Al}_2\text{O}_3/\text{YAG}$ ceramic composite, and the spatial distributions of residual strains in both constituent phases were mapped by the FEM calculation.

2 Experimental

2.1 Material system

The $\text{Al}_2\text{O}_3/\text{YAG}$ ceramic composites were fabricated by a Bridgman method at Ultra-high Temperature Materials Research Center, Yamaguchi, Japan. The fabrication procedure has been described in more detail elsewhere [10].

The surface morphology on the face parallel to the solidification direction of the fabricated specimen is shown in Fig. 1, in which the alumina and YAG phases correspond to the dark and the light phases, respectively.

From the observation of CT images, it has been shown that the single crystal Al_2O_3 and YAG phases are three-dimensionally continuous and entangled structure with narrower lamellar spacing in this composite. The entangled domain was of the same order as the lamellar spacing [11]. The alumina and YAG crystals on the face parallel to the solidification are elongated in comparison with those on the face perpendicular to it as observed in Fig. 1.

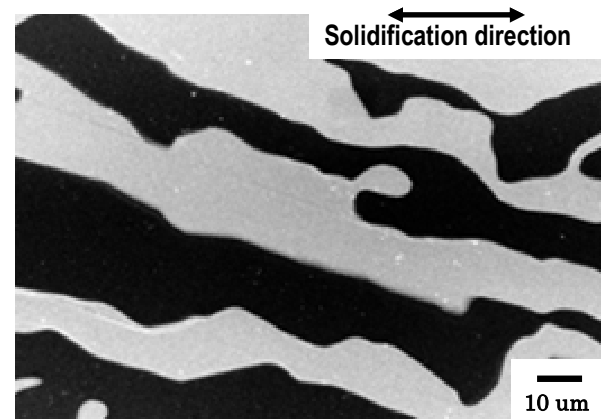


Fig. 1. Surface morphology of $\text{Al}_2\text{O}_3/\text{YAG}$ ceramic composite on the face parallel to the solidification direction, the dark and light phases in this composite correspond to the Al_2O_3 and YAG phases respectively.

A cubic specimen with edge dimension of 10 mm was used to measure the residual strains. During the strain measurement, the X-ray beam was positioned toward the center area of the specimen. The mutually perpendicular directions in the specimen shown in Fig. 2, were assigned S_1 , S_2 , and S_3 (principal direction in a specimen system), respectively.

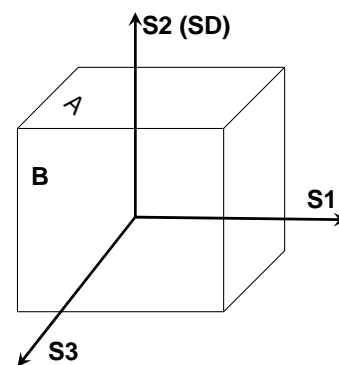


Fig. 2. Schematic illustration of the specimen geometry and the faces for the X-ray strain measurement, SD: solidification direction.

In order to measure the un-strained lattice parameter, d_0 , the sheets with a dimension of $10^1 \times 10^w \times 0.6^t \text{ mm}$ were cut from the corresponding planes of the bulk composites, and then the Al_2O_3 phase in composite was removed by a deoxidization in carbon container in vacuum at 1873 K for 7.2 ks. The depth of the Al_2O_3 -removed region in the thickness direction of the sample was around 250 μm , being around 8 to 25 times the thickness of the YAG (around 10~30 μm). Surface morphologies in such specimen were examined by scanning electron

**EXPERIMENTAL AND NUMERICAL INVESTIGATIONS ON THE RESIDUAL STRAINS OF YAG PHASE
IN DIRECTIONALLY SOLIDIFIED EUTECTIC Al_2O_3 /YAG CERAMIC COMPOSITE**

microscopy (SEM), as shown in Fig. 3. The specimen prepared in this way, hereafter noted as the YAG skeleton specimen, was used as the un-strained reference specimen for X-ray strain measurement. The lattice spacing d_0 of the skeleton YAG determines the sign and magnitude of strains, as will be shown later.

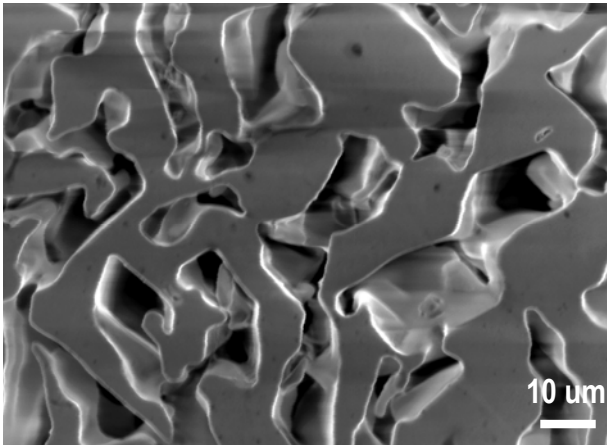


Fig. 3. Surface morphology of YAG skeleton specimen obtained on the face A perpendicular to the solidification direction.

The extent of preferred growth orientations on each surface of specimen was determined by X-ray diffraction (diffraction vector is normal to the surface of specimen). An example of diffraction pattern measured with $CuK\alpha_1$ irradiation on the B face parallel to the solidification direction is presented in Fig.4. Evidently, the $\{001\}$ diffractions for Al_2O_3 and $\{211\}$ diffractions for YAG are found, which indicates that the $\{001\}$ Al_2O_3 and $\{211\}$ YAG crystals preferentially arrange themselves along the S_3 axis.

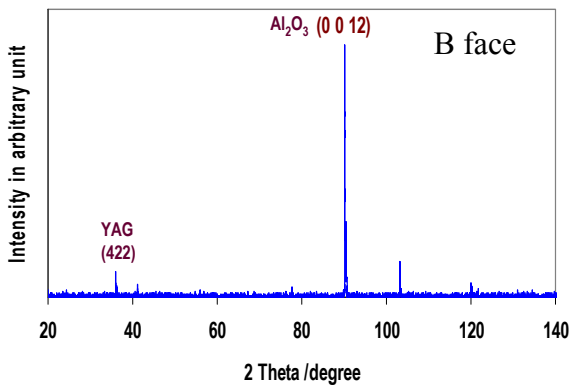


Fig. 4. Diffraction pattern measured with $CuK\alpha$ irradiation on the B face.

This is consistent with the crystallographic relationship revealed in the earlier work [11] that the

crystallographic orientation between the two constituent phases are:

$$S_3 // [0001]_A // [1 \bar{1} 2]_Y; S_2 // SD // [\bar{1} 0 10]_A // [\bar{1} 1 1]_Y$$

It should be noted that, according to the pole figure analysis carried in this work, the preferred growth orientation slightly tilts from the normal of the corresponding specimen surface by 3° - 4° . The composite specimens have been solidified along the S_2 direction. Because of single crystal-like structure, the method for the measurement of residual strain in polycrystal materials is not applicable. The detailed method for the present DSE specimen is described in following sections.

2.2 X-ray diffraction

The X-ray strain measurements with $CuK\alpha$ irradiation were performed on the two faces: parallel and perpendicular to the solidification direction. In order to find the diffraction plane which is suitable for the X-ray strain measurement, first X-ray diffraction patterns were obtained from the precursor powder of Al_2O_3 and YAG phases as shown in Fig. 5.

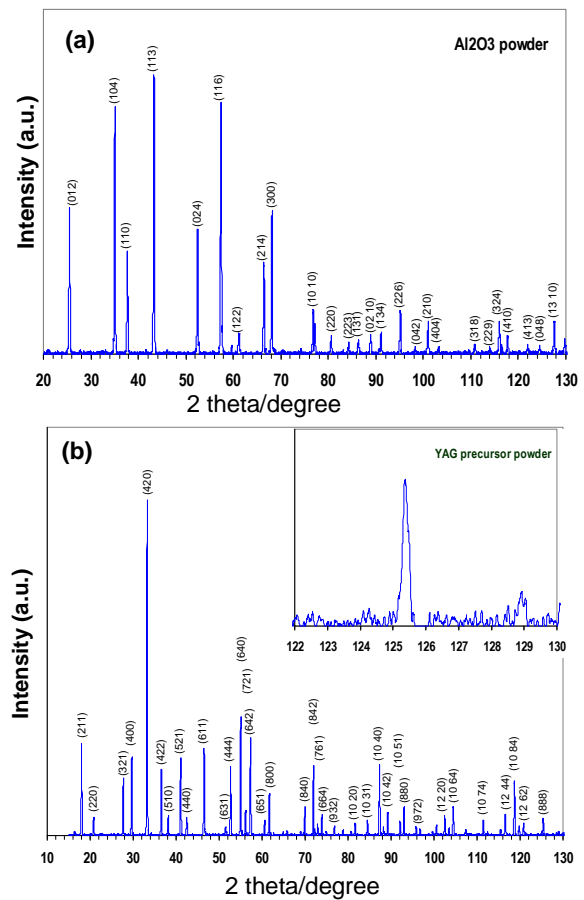


Fig. 5. X-ray diffraction patterns for the Al_2O_3 and YAG precursor powder.

It is obvious that Al_2O_3 phase belongs to the hexagonal system (Fig. 5(a)), and YAG belongs to the cubic system (Fig. 5(b)).

If the diffraction peak at higher angle is used, the estimated strain-value is more accurate. However, based on a crystal diffraction structure index program (ICDD-DD view), for the high angle peaks, the database of the YAG phase is only available up to 90° in 2θ . In the present work, the indices of interesting high angle diffractions were obtained by combining the Bragg law with the plane-spacing. Then, the diffractions of $\{888\}$ ($2\theta=125.38^\circ$) for YAG phase were chosen for strain measurement. This angular position was derived from the diffraction patterns of YAG precursor powder as shown in the upper right of Fig. 5(b).

The stress states in polycrystalline materials which contain many crystal grains with random orientations in an X-ray irradiation area, can be measured by using the $\sin^2\psi$ method [12-13]; however, this method is not applicable to the materials used in the present work, since the identical crystallographic plane can not be found in this material which has a strong texture. Nevertheless, the fundamental principal for X-ray strain measurement is still same, which starts from the measurement of the interplanar spacing, d .

The interplanar spacing, d , for a particular set of hkl planes of a given phase can be measured from the corresponding peak in the diffraction pattern with Bragg's law:

$$d = \frac{\lambda}{2 \sin \theta_B} \quad (1)$$

where θ_B was the Bragg angle and obtained from the measurement of $K\alpha_1$ peak position, λ wave length of $\text{CuK}\alpha_1$ irradiation. XRD patterns were measured using a Rigaku X-ray diffractometer (RINT 2000 series, Model D/max-2200) with a four-circle goniometer (ϕ , ψ , ω , 2θ).

The X-ray diffraction setup and specimen mounting are shown in Fig. 6. The specimen can rotate in its own plane about an axis (A-A') normal to its surface, and about a horizontal axis (B-B'). The horizontal axis lies in the specimen surface and it is initially adjusted by rotation about the diffractometer axis (C-C'), to realize the equal angles with the incidence and diffraction beams. After such an adjustment, the horizontal axis was fixed (no further rotation about the diffractometer axis).

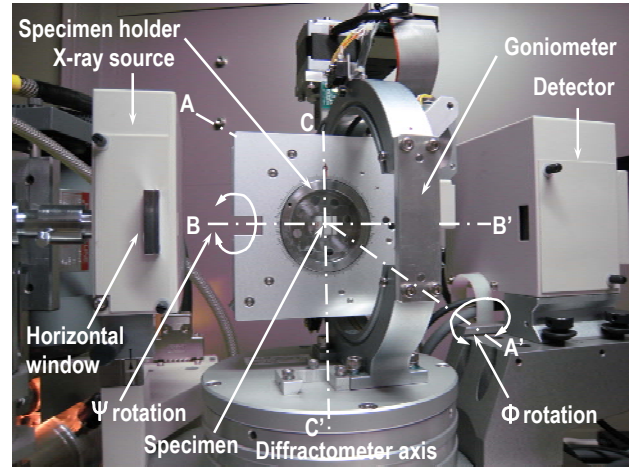


Fig. 6. X-ray diffractometer with four-circle goniometer for strain measurement.

In order to know the principal residual strains (normal to each surface) in this composite, two coordinate systems were defined, namely, the laboratory coordinate system and specimen coordinate one. The relationship between the two coordinate systems is presented in Fig. 7.

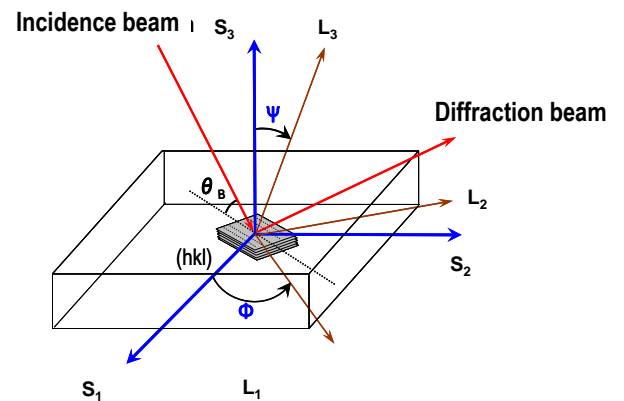


Fig. 7. The laboratory coordinate system and the specimen coordinate system, and the definition of ϕ and ψ angles in the present specimen.

Fig. 7 shows a laboratory coordinate system L_i with respect to a specimen coordinate one S_i , and the definition of ψ and ϕ angles. The direction of the incident beam with respect to the specimen's coordinates was determined by these two angles: ψ and ϕ (see Fig. 6 and Fig. 7). The specimen was mounted onto a goniometer head that was used to position a specimen in the X-ray beam and was oriented with respect to the specimen coordinate system (S_i) so that the ϕ axis coincide with the normal of the surface of the specimen throughout the experiment (Fig. 7). In Fig. 6, the ψ angle is zero

EXPERIMENTAL AND NUMERICAL INVESTIGATIONS ON THE RESIDUAL STRAINS OF YAG PHASE IN DIRECTIONALLY SOLIDIFIED EUTECTIC Al_2O_3/YAG CERAMIC COMPOSITE

when the surface of specimen is vertical and has a value of 90° when the surface of specimen is in the horizontal position. Both angles ψ and ϕ can be extracted from the pole figure analysis.

During the X-ray strain measurement, a $CuK\alpha$ irradiation was used at 40 kV and 200 mA. The relevant diffractometer conditions are summarized in Table 1. To ensure that only reflections in the vertical plane of the diffractometer were being measured, a 2.0 mm horizontal window was placed at the position after the incidence slit.

Table 1. X-ray diffractometer conditions for residual strain measurement.

Parameter	Condition
Equipment	Rigaku XRD: $CuK\alpha$ X-ray tube; four circle goniometer
Power	8 kW; 40 kV, 200 mA
Radiation	$CuK\alpha$, $\lambda=1.540562 \text{ \AA}$
Reflection	{8 8 8}
2θ range	$125.1-125.8^\circ$
Divergence slit	0.25° ; 2.0 mm horizontal window
Soller slit	0.25°
Receiving slit	0.15 mm
Source-to-specimen distance	185 mm
Scans	Step: 0.004° ; $2\theta/\text{step}$; 2.4s/step

The direction of strain with respect to the specimen is always along the bisector of the incident and diffracted beams, namely, along the L_3 axis (Fig. 7). Actually, the L_3 is normal to the diffraction planes. Thus, by tilting the sample relative to the incident beam, this bisector can be made to make various angles, ψ , with the normal to the specimen surface. The direction of strain on the laboratory coordinate system (L_i), is defined by the angle ψ and by the angle ϕ that the plane of the normal of the specimen's surface (S_3) and the normal of diffraction plane (L_3) makes with a arbitrary direction in the specimen surface. In this work, the normal of the S_1 was chosen as the reference direction for angle ϕ . If strain measurements are carried using at least six independent directions defined by ϕ and ψ , all the components of the strain tensor for the phase can be obtained by the multiple linear analysis. These strain components measured from the specific hkl planes are averaged over the volume of the specimen irradiated by the X-ray beam. For a simpler procedure, requiring less data points, may be used for the determination of principal strains. In that case, it required at least 3 independent diffractions.

The X-ray pole figure analysis was performed on the family of {888} diffraction using the Shulz reflection method [13] to determine the locations of the diffraction planes which were used to measure the residual strain in YAG phase.

Knowing the complete orientation of each diffraction on the pole figure, and rotating the goniometer by a combination of ϕ and ψ degrees, a particular diffraction normal was brought into the diffraction plane. Then a $2\theta/\theta$ scan was collected from each accessible member of the YAG {888} family of diffraction.

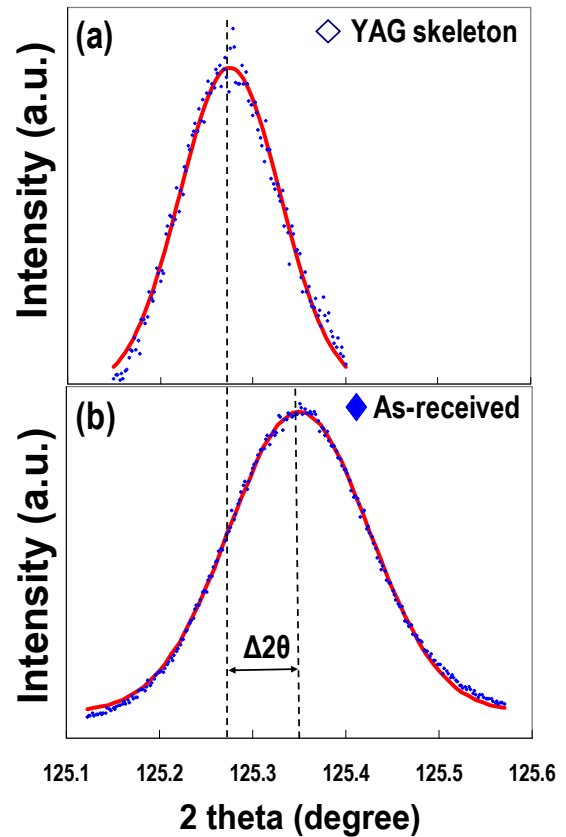


Fig. 8. Diffraction peak profiles (data points) measured from YAG 888 family of diffraction on the face B parallel to the solidification for the as-received composite and YAG skeleton specimen and their fitting lines (solid line: fit to Gaussian function).

The peak profiles for both the as-received and skeleton specimens were obtained in the range of $125.1-125.8^\circ$ for YAG {888} family. The result is shown in Fig. 8. The peak profile of the YAG phase in the composite (Fig. 8(b)) is broadened and shifted to larger 2θ in comparison with that of the skeleton YAG (Fig. 8(a)). The quantitative peak broadenings were expressed as FWHM (full width at half maximum) in Fig. 9. The 2θ positions were

determined by a fitting of the background-subtracted peak to the Gaussian function. The fit profiles are shown with solid lines in Fig. 8.

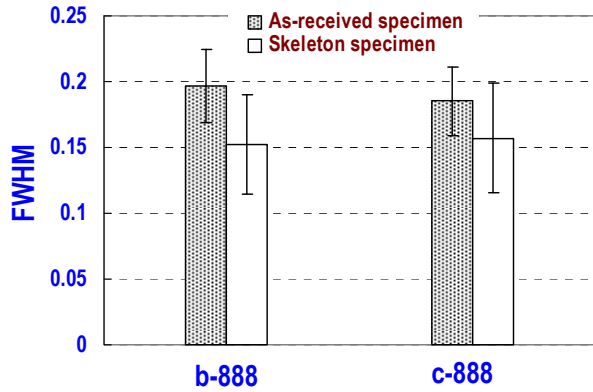


Fig. 9. Peak broadening measured from the full width at half maximum of diffraction peak profiles.

The peak shift and broadening observed in the as-received composite (Fig. 8) implied the existence of residual strains and their inhomogeneous distribution. Based the diffraction law, it would be clear that lattice spacing of YAG phase in the as-received composite is smaller than that of the YAG skeleton specimen, indicating the YAG phase in composite has the compressive strains.

2.3 Finite element method (FEM) simulation

Using the software Adobe illustrator with MARC/Mental™, an image-based FEM simulation was conducted to calculate the distribution of the residual strains on face A in this composite.

Fig. 10(a) shows the FEM model with boundary conditions for calculation of residual strains. The model was constructed based on the real microstructure observed by SEM, as shown in Fig. 10(b). The size of the composite for the model was 0.18×0.21 mm. The number of elements in model was 58673. The meshes for the portion picked up from Fig. 10(b) are shown in Fig. 10(c). For the calculation of thermal mismatched strains, a given temperature difference between the strain-generated temperature (1423K, shown later) and room temperature was applied to each mesh.

In this model, as a first approximation, the temperature dependence of CTE and Young’s modulus were taken from our previous work [14]; $E^Y=299-0.0180T$ (GPa), $E^A=423-0.0474T$ (GPa), $\alpha^Y=6.09+0.00117T$ ($\times 10^{-6}/K$), $\alpha^A=6.50+0.00146T$ ($\times 10^{-6}/K$), where Y and A refer to YAG and Al₂O₃, respectively. The poisson’s ratios are 0.23 for Al₂O₃ phase and 0.25 for YAG phase, respectively.

Inputting such values into FEM model, the in-plane residual strains caused by mismatch of CET were estimated.

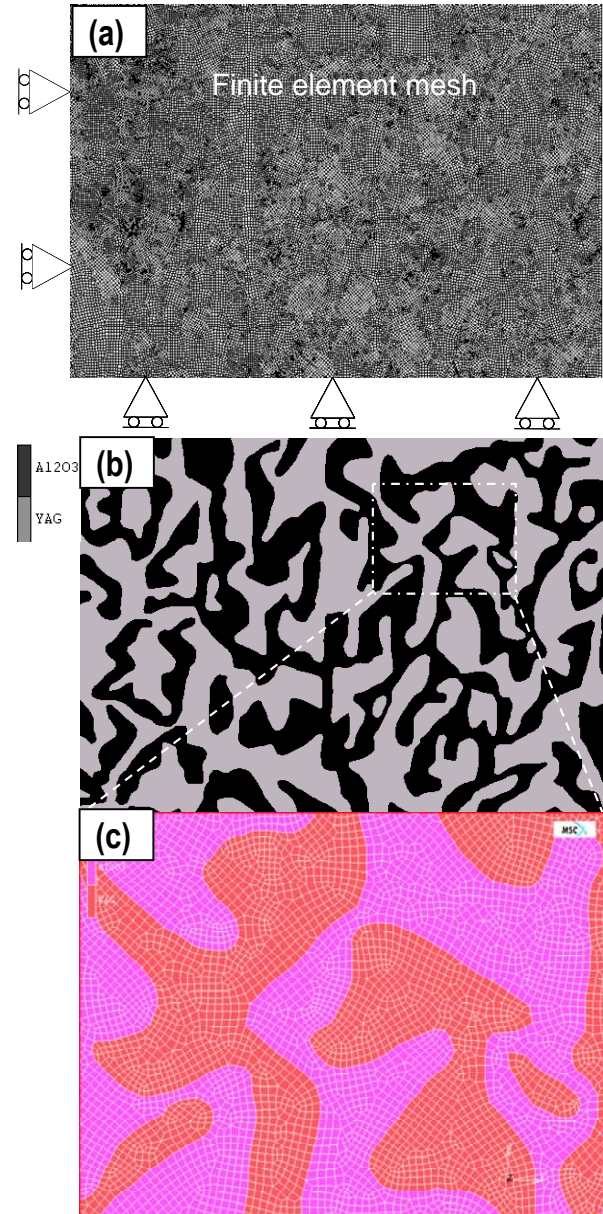


Fig. 10. The constructed finite element mesh based on the image of face A, the number of elements is 58673.

3 Result

3.1 Residual strains by X-ray diffractions

The total strain, $e_{hkl}^{\phi\psi}$, was obtained from different crystallographic planes ($d_{hkl}^{\phi\psi}$) and the unstrained lattice parameter (d_0) by following equation:

**EXPERIMENTAL AND NUMERICAL INVESTIGATIONS ON THE RESIDUAL STRAINS OF YAG PHASE
IN DIRECTIONALLY SOLIDIFIED EUTECTIC Al_2O_3/YAG CERAMIC COMPOSITE**

$$e_{hkl}^{\phi\psi} = \frac{d_{hkl}^{\phi\psi} - d_0}{d_0} \quad (2)$$

where $e_{hkl}^{\phi\psi}$ is the measured strain for diffraction (hkl) located at ϕ and ψ (along the L_3 direction). The measured residual strains at different diffraction locations on both faces are tabulated in Table 2.

Table 2. Residual strains measured at different locations.

	Orientation of diffraction		Interplanar spacing d (nm)	Strain ($\times 10^4$) ϵ
	ϕ (°)	X (°)		
A face	270	47	0.866796	-3.3
	32.2	33.8	0.866905	-2.0
	121	67.7	0.866905	-2.0
	191	75	0.866791	-3.3
	64.5	61.2	0.866831	-3.4
B face	202	62.2	0.86703	-3.5
	313	31.1	0.866858	-3.9
	180	55.4	0.868342	-4.3

Then, using the relationship between the two coordinate systems, the strain tensor ϵ_{ij} in the specimen coordinate system (S_i) can be determined by following equation:

$$e_{hkl}^{\phi\psi} = a_i a_j \epsilon_{ij} \quad (3)$$

where a_i is the direction cosine between the (hkl) diffraction and axis i . It should be emphasized that the ϵ_{ij} depends on the orientation of the laboratory coordinate system with respect to the specimen coordinate one if the sample is textured. Using at least six measured d -spacings and combining Eqs. (2) with (3), the strain tensor can be determined with generalized least-squares method [15] by:

$$e_{hkl}^{\phi\psi} = (\epsilon_{11} \cos^2 \phi + \epsilon_{12} \sin 2\phi + \epsilon_{22} \sin^2 \phi) \sin^2 \psi + \epsilon_{33} \cos^2 \psi + \epsilon_{13} \cos \phi \sin 2\psi + \epsilon_{23} \sin \phi \sin 2\psi \quad (4)$$

However, for the YAG {888} family, less than six diffractions were found in the present work. Then, we neglected the existence of shear strain components and estimated just the principal residual strains. The estimated principal residual strains in the specimen coordinate system are shown in Fig. 11.

The residual strain analysis by generalized least square method showed that principal residual strains of YAG phase in composite were in the range from $-2.19 \pm 0.32 (\times 10^{-4})$ to $-4.22 \pm 0.08 (\times 10^{-4})$ commonly

for both faces parallel and perpendicular to the solidification direction.

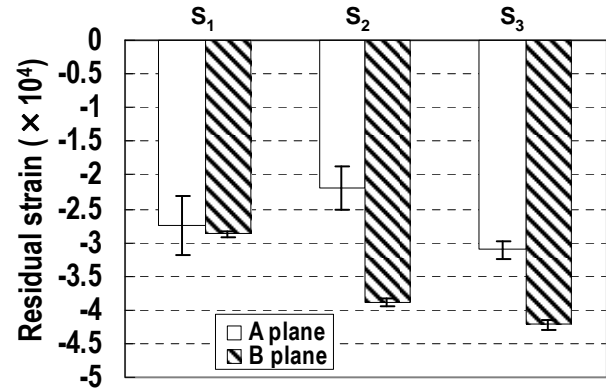


Fig. 11. The principal residual strains measured from YAG 888 family of diffractions on both A and B faces.

The standard deviations in the measured strain were obtained from the variances in the diffracted peak position. To facilitate a matrix formulation of the least-squares procedure the following definitions were made in Eq.(4):

$$\epsilon_1 = \epsilon_{11}, \quad \epsilon_2 = \epsilon_{22}, \quad \epsilon_3 = \epsilon_{33},$$

$$\epsilon_4 = \epsilon_{12}, \quad \epsilon_5 = \epsilon_{13}, \quad \epsilon_6 = \epsilon_{23},$$

The variance in the strains may be calculated from the variance in each of the measured strains

$$\text{var}(\epsilon_j) = \sum_{i=1}^n \left(\frac{\partial \epsilon_j}{\partial e_i} \right)^2 \text{var}(e_i) \quad (5)$$

The variance in e is computed from the variance in 2θ by following equation.

$$\text{var}(e_i) = \left(\frac{1}{d_0} \right)^2 \left(\frac{\pi}{180} \right)^2 \left(\frac{\lambda \cos \theta_i}{2 \sin^2 \theta_i} \right)^2 \frac{\text{var}(2\theta)}{2} \quad (6)$$

Where $\text{var}(2\theta)$ is given by the errors in 2θ which can be determined from nonlinear least-squares fits of peaks to analytical functions. The standard deviations were given by the square roots of the variances.

3.2 Residual strains by FEM calculation

In order to calculate the residual strains caused by CTE mismatch, it is necessary to know the strain-generated temperature, at which the accumulation of elastic strains begins [9]. Since the elastic strains were generated by the thermal expansion mismatch at temperatures below the eutectic temperature, an

approximate value of this temperature can be estimated from the minimum temperature necessary to activate the slip systems in the eutectic crystal phases.

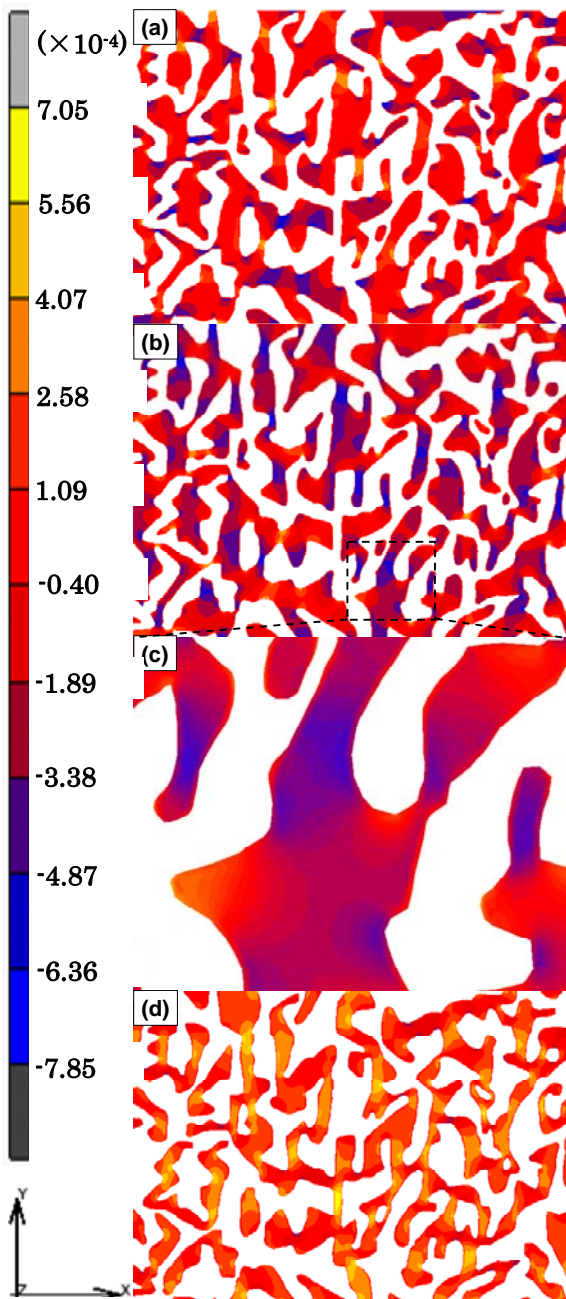


Fig. 12. Calculated distribution of residual strains of (a) YAG phase in x direction, (b) YAG phase in y direction, (c) YAG phase in y direction at high magnification, showing the influence of local morphology on the residual strain distribution and (d) Al_2O_3 phase in y direction.

In the present calculation, the onset temperature of dislocation slip in prismatic and pyramidal planes

in Al_2O_3 , 1423 K, was taken as the strain-generated temperature, which has been used for analysis of residual stresses in $\text{Al}_2\text{O}_3/\text{YSZ}$ composite [9]. The calculation results of residual strain are presented in Fig. 12. From the Fig. 12, it can be seen that: (1) the distribution of residual strains is non-uniform and quite dependent on the local morphology; (2) the thinner region of YAG has the higher strain intensity than that of thicker one. As will be shown later in detail, the average residual strain calculated by FEM model ($-1.71 \pm 0.88 (\times 10^{-4})$) was comparable with those principal residual strains by X-ray measurements (minimum value: $-2.19 \pm 0.32 (\times 10^{-4})$, maximum value: $-4.22 \pm 0.08 (\times 10^{-4})$).

4. Discussion

The principal residual strains measured from the family of YAG {888} diffraction (Fig. 11), showed that YAG phase in composite is in compression. Such a result was common for faces A and B and for the directions S_1 , S_2 and S_3 . Since the coefficient of thermal expansion of the YAG phase is lower than that of the alumina phase, the alumina will contract more during cooling from the processing temperature to room one, giving a compression strain to the YAG phase. This result was accounted for by the FEM calculation as shown in Fig. 12. In this section, the factors affecting on the estimated residual strains are discussed.

4.1 The influence of un-strained lattice parameters on the X-ray strain measurement

Small variations in d_0 can greatly affect on the accuracy of the strain measurement, especially when the difference in coefficient of thermal expansion between the constituent phases is small as in the present composite. Dickey et al measured the residual stress in the $\text{Al}_2\text{O}_3/\text{YAG}$ composite whose microstructure is finer than that of the present composite by X ray diffraction. They concluded that the residual strain in their composite is nearly zero within the error [8]. Torii et al [16] investigated the residual strains in the composite same as in the present study by neutron diffraction. Their result indicated that the YAG phase was in tension and the strain was on the order of 10^{-4} . In these studies, the d_0 -values were obtained from either pulverized powders or the sintered composites due to the difficulties of the preparation of the strain free reference sample. For accurate measurement, it is needed to use the strain free reference specimen taken out of the composite, otherwise the difference

in lattice parameter between the strain free- and strained states is different from that of the practical composite. In the present work, the YAG phase extracted from the composite was prepared as the thermally induced residual strain-free specimen and the result comparable with the calculation result could be obtained.

4.2 The influence of morphology on the distribution of residual strains

It is noted that the residual strain-values were different from direction to direction. The residual strains along the c axis were somewhat higher than that of other axes. Two possible reasons might be responsible for such a difference: (i) anisotropy in CTE of Al_2O_3 , a higher CTE in c-axis has been observed in comparison to that of other axes [9]; (ii) difference in morphology of constituent phases between faces A and B, Al_2O_3 and YAG phases on face B are elongated along the solidification direction in comparison to that of face A. The distribution of residual strains is significantly affected by the morphology of constituent phases as discussed below.

The mapping of residual strains by FEM calculation in Fig.12, shows that the YAG and Al_2O_3 have compressive and tensile strains respectively, and a non-uniform distribution of the residual strains is found in both phases. Namely, the residual strain is different from position to position, due to the variation of local morphology such as thickness, curvature and local volume fraction (Fig. 12(c)). The high and low residual strain regions coexist within YAG and Al_2O_3 phases, while the average residual strain (-1.71×10^{-4}) in YAG phase of composite is not so different from the measured one.

The $CuK\alpha 1$ radiation used for the X-ray strain measurement had a maximum penetration depth of about 125 μm (for 90% attenuation), which was calculated by the method in the literature [12]. Since the X-ray penetration depth (125 μm) (and therefore the X-ray irradiated volume) was large enough compared with the phase dimensions (10-30 μm), the strain gradients and local morphology of constituent phase shown in Fig.12(c) were judged to be averaged in the X-ray measurement of residual strains. Therefore, it can be understood that the value of residual strains in the present study determined by the X-ray diffraction is a mean value in the X-ray irradiated volume, while it is distributed depending on the local morphology of the YAG phase. On the other hand, it is emphasized that the peak

broadening is strongly affected by such distributed residual strains, as follows.

The non-uniform distribution of residual strains induced by the complex local morphology is the major cause for the broadening of diffraction peak as shown in Fig. 8 and Fig.9. Namely, in the X-ray irradiated volume, the diffraction planes are slightly mis-oriented to each other. The relation between the peak broadening and non-uniformity of the strain is expressed by differentiating the Bragg law [13]:

$$b = -2 \frac{\Delta d}{d} \cdot \tan \theta \cdot \frac{180}{\pi} \quad (7)$$

where b is the extra broadening, over and above the instrumental breadth of the profile. The fractional variation in plane spacing ($\Delta d/d$) calculated from the observed broadening varied from 1.3×10^{-4} to 1.9×10^{-4} on face A and B respectively. These values of $\Delta d/d$, are comparable with the calculated wide distribution of residual strains in the YAG phase of composite (Fig. 12).

4.3 The influence of deformation behaviour of constituent phases on the residual strains

A slight difference in residual strain between the X-ray measured ($-2.19 \pm 0.32 (\times 10^{-4})$) and the FEM calculated ($-1.71 \pm 0.88 (\times 10^{-4})$) may be attributed to the following reason.

In present work, we assumed that the residual strains were generated at 1423 K. The residual strains in practical composite are, however, not necessarily relaxed completely by the plastic deformation of Al_2O_3 phase (dependent on the temperature difference and cooling rate [17]). Even the temperature is higher than 1423 K, the time for specimen retained at high temperatures is not so long during cooling, since the specimens are cooled compulsorily from the bottom during fabrication. In this case, the practical residual strains existing in the composite will be underestimated by FEM calculation when 1423 K is used as the onset temperature for the strain accumulation. For exact estimation of the onset temperature for residual strain accumulation, further study is needed.

5. Summary

The residual strains of YAG phase in directionally solidified eutectic $Al_2O_3/Y_3Al_5O_{12}$ (YAG) ceramic composite were estimated by X-ray diffraction technique and finite element method (FEM). The X-ray strain measurements with $CuK\alpha$ irradiation were performed on the two faces:

perpendicular (face A) and parallel (face B) to the solidification direction, where the YAG skeleton specimen without the Al_2O_3 phase was taken as the un-strained specimen (reference). The main results are summarized as follows:

(1) The residual strains measured by X-ray diffraction showed that principal residual strains of YAG phase in composite were ranging from $-2.19 \pm 0.32 (\times 10^{-4})$ to $-4.22 \pm 0.08 (\times 10^{-4})$ commonly for both faces parallel and perpendicular to the solidification direction. The experimental results were accounted for by the FEM simulation.

(2) An image-based FEM simulation was performed on the face A. The calculated residual strain by FEM model, is $-1.71 \pm 0.88 (\times 10^{-4})$, which are comparable to the experimental results. The mapping of residual strains of YAG phase also revealed that the residual strains are strongly dependent on the local morphology of YAG Phase. The experimentally observed wide distribution of residual strains in YAG phase was accounted for by the variation of local morphologies (microstructure complexity) based on the FEM analysis.

Acknowledgements:

The authors would like to give their sincere thanks to the financial support of this work by the Japan Society for the Promotion of Science (JSPS).

References

- [1] Hirano K. "Application of eutectic composites to gas turbine system and fundamental fracture properties up to 1700 °C". *J. Europ. Ceram. Soc.*, Vol. 25, No. 8, pp 1191-9, 2005.
- [2] Nakagawa N., Ohtsubo H., Mitani A., Shimizu K. and Waku Y. "High temperature strength and thermal stability for melt growth composite". *J. Europ Ceram Soc.*, Vol. 25, No. 8, pp 1251-7, 2005.
- [3] Ashbrook R. L. "Directionally solidified ceramic eutectics". *J. Am. Ceram. Soc.*, Vol. 60, No. 9-10, pp 428-435, 1977.
- [4] Sayir A. and Farmer S. C. "The effect of the microstructure on mechanical properties of directionally solidified $\text{Al}_2\text{O}_3/\text{ZrO}_2(\text{Y}_2\text{O}_3)$ eutectic". *Acta Mater.*, Vol. 48, pp 4691-7, 2000.
- [5] Ishikawa T., Sakata S. and Mitani A. "Durable, Ultraluminous structure for incandescent, high-powder whit-LED". *Int. J. Appl. Ceram. Techno.*, Vol. 3, No. 2, pp 144-149, 2006.
- [6] Brewer L. N., Peascoe, R. A. Hubbard C.R. and Dravid V.P. "Residual stress distribution in the solid solution eutectic $\text{Co}_{1-x}\text{Ni}_x/\text{ZrO}_2(\text{CaO})$ ". *J. Am. Ceram. Soc.*, Vol. 86, No. 12, pp 2188-94, 2003.
- [7] Dickey E. C. and Dravid V. P. "Interlamellar residual stresses in single grain of $\text{NiO-ZrO}_2(\text{cubic})$ directionally solidified eutectics". *J. Am. Ceram. Soc.*, Vol. 80, No. 11, pp 2773-80, 1997.
- [8] Dickey E.C., Frazer C.S., Watkins T. R. and Hubbard C.R. "Residual stresses in high temperature ceramic eutectics". *J. Eur. Ceram. Soc.*, Vol. 19, No. 13-14, pp 2503-509, 1999.
- [9] LLorca J. and Orera V. M. "Directionally solidified eutectic ceramic oxides". *Progress in Materials Science*, Vol. 51, pp 711-809, 2006.
- [10] Waku Y. Otsubo H. Nakagawa N. and Kohtoku Y. "Sapphire matrix composites reinforced with single crystal YAG phases". *J. Mater. Sci.*, Vol. 31, No. , pp 4663-70, 1996.
- [11] Yasuda H., Ohnaka I., Mizutani Y., Morikawa T., Takeshima S., Sugiyama A., Waku Y., Tsuchiyama A., Nakano T. and Uesugi K. "Three-dimensional observation of the entangled eutectic structure in the $\text{Al}_2\text{O}_3\text{-YAG}$ system". *J. Euro. Ceram. Soc.*, Vol. 25, pp 1397-1403, 2005.
- [12] Cullity B. D. "*Elements of X-ray diffraction*". 2nd edition, Addison Wesley, Reading, MA, 1978.
- [13] Noyan I. C. and Cohen J. B. "*Residual stress: Measurement by Diffraction and Interpretation*". 1st edition, Springer-Verlag, New York, 1987.
- [14] Ochiai S., Ueda T., Sato K., Hojo M., Waku Y., Sakata S., Mitani A., Takahashi T. and Nakagawa N. "Elastic modulus and coefficient of thermal expansion of $\text{Al}_2\text{O}_3/\text{YAG}$ composite at ultra high temperatures". *Mater. Sci. Res. Int. Special Technical Publication-2, the Society of Materials Science*, Kyoto, Japan, pp. 282-285, 2001.
- [15] Winholtz R. A. and Cohen J. B. "*Generalized Least-squares determination of triaxial stress states by X-ray diffraction and the associated errors*". *Aust. J. Phys.*, Vol. 41, pp 189-99, 1988.
- [16] Torii S., Kamiyama T., Oikawa K., Waku Y. and Fukunaga T. "*Strain measurement of the directionally solidified eutectic $\text{Al}_2\text{O}_3/\text{Y}_3\text{Al}_5\text{O}_{12}$ (YAG) ceramic by neutron diffraction*". *J. Euro. Ceram. Soc.*, Vol. 25, pp 1307-1311, 2005.
- [17] Ochiai S., Sakai Y., Sato K., Tanaka M., Hojo M., Okuda H., Waku Y., Nakagawa N., Sakata S., Mitani A., Takahashi T. "*Fracture characteristics of $\text{Al}_2\text{O}_3/\text{YAG}$ composite at room temperature to 2023 K*". *J. Euro. Ceram. Soc.*, Vol. 25, No. 8, pp 1241-9, 2005.